IEEE Access
Multidisciplinary ⋮ Rapid Review ⋮ Open Access Journal

Received 23 March 2024, accepted 21 April 2024, date of publication 1 May 2024, date of current version 8 May 2024.

Digital Object Identifier 10.1109/ACCESS.2024.3395926

RESEARCH ARTICLE

Dynamic Inductance Gradient Analysis of Series-Enhanced Four-Rail Electromagnetic Launcher

BO-LIN CAI[1], GANG FENG[2], AND KE-FENG YANG[1]
[1]Graduate College, Air Force Engineering University, Xi'an 710051, China
[2]Air and Defense College, Air Force Engineering University, Xi'an 710051, China
Corresponding author: Bo-Lin Cai (2151179067@qq.com)

ABSTRACT To accurately describe the dynamic inductance gradient during the operation process of the series enhanced four-rail electromagnetic rail launcher, an equivalent geometric model based on skin depth is constructed. The influence of armature motion on current diffusion in the rail is considered, and the velocity skin effect is derived. Combined with Biot-Savart Law, an analytical calculation method for dynamic inductance gradient is proposed, and an experimental platform for the series-enhanced four-rail electromagnetic launcher is built, Calculate the dynamic inductance gradient of the experimental device and compare it with the eddy current field simulation calculation, demonstrating the correctness of the proposed analytical method for calculating the dynamic inductance gradient. Analyze the influence of armature motion on the system inductance gradient, and obtain that the initial velocity of armature launching is small, and the distribution of rail current is affected by the current skin effect and related to the current frequency. As the armature velocity increases, the distribution of current in the middle section of armature launching is affected by the velocity skin effect, The skin depth decreases and the dynamic inductance gradient decreases. As the armature speed increases, the dynamic inductance gradient gradually decreases and tends to stabilize in the accelerated stage of armature launching.

INDEX TERMS Electrical launching, series-enhanced four-rail electromagnetic launcher, dynamic inductance gradient, velocity skin effect, electromagnetic rail launcher velocity test, B-dot probe.

I. INTRODUCTION

Electromagnetic launch technology is a launch technology that utilizes an armature driven by the Lorentz force in a strong magnetic field to accelerate a load to ultra-high speeds in milliseconds [1]. It is characterized by the ability to break through the gunpowder launch speed limit to obtain higher load kinetic energy, and has the advantage of launching the load at a controllable speed [2]. In order to prolong the service life of the launcher and inhibit fusion wear [3], scholars have proposed the use of back-field rails to enhance the magnetic field in the chamber, which allows the electromagnetic launcher to use a smaller current while obtaining the same thrust. Series-enhanced four-rail electromagnetic launcher [4] adopts this design concept by distributing the four rails in a 90° circumferential array around the armature, with the main and enhanced rails stacked accordingly. While providing large thrust, the magnetic fields of the four poles cancel each other on the bore axis, which can better meet the requirements of launching intelligent projectiles.

Inductance gradient is one of the important parameters of series-enhanced four-rail electromagnetic launcher, which is related to the load exit kinetic energy and system launch efficiency. Scholars at home and abroad have conducted a lot of research on the inductance gradient calculation methods and influencing factors, Grover and Grover [5] studied the calculation method of inductance gradient when the current is completely diffused in the rail at low frequency, and Kerrisk [6] proposed the formula of inductance gradient when the current is concentrated in the surface of the rail in the

The associate editor coordinating the review of this manuscript and approving it for publication was Wei Xu.

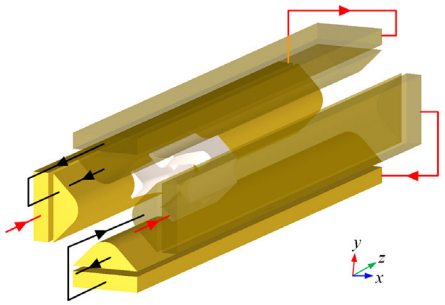

FIGURE 1. Three-dimensional diagram of a series enhanced four-rail electromagnetic launcher.

high-frequency state during the pre-launch period by taking the size of the rail into consideration. Li et al. [7] used Ansys Maxwell software simulation to calculate the system energy increment and used the principle of virtual work to calculate the average inductance gradient over the distance of armature motion in a short period of time. Ren et al. [8] derived the analytical calculation method of inductance gradient in high frequency state by Biot-Savart Law. The above methods cannot accurately describe the transient inductance gradient during the launching process, and the inductance gradient changes dynamically during the actual launching process when the current and magnetic field diffuse in the orbit affected by the armature motion. Peng et al. [9] proposed a time-varying inductance gradient analytical calculation method to calculate the common dual-rail electromagnetic launch by considering the skin depth and the principle of magnetic energy equivalence, and Zhai et al. [10] introduced the velocity frequency to calculate the dynamics of the dual-rail electromagnetic launcher, but the inductance gradient could not be obtained directly through simulation. Ghassemi et al. [11] used mechanical analysis to establish a dynamic model of inductance gradient based on the change of rail spacing, but did not consider the effect of current diffusion in the rail on the inductance gradient. Li et al. [12] used finite element simulation to calculate the inductance gradient at different frequencies from the instantaneous frequency of the current, but the calculation is time-consuming.

In order to obtain the accurate inductance gradient of the enhanced four-rail electromagnetic launcher during the launching process, this paper considers the effect of armature motion, establishes an equivalent geometric model based on skin depth, deduces the velocity skin effect, proposes an analytical calculation method of the dynamic inductance gradient in combination with Biot-Savart Law, builds a series-enhanced four-rail electromagnetic launcher test platform, computes the dynamic inductance gradient of the test device, compares it with the eddy-current field simulation calculation, and analyzes the effect of armature motion on the inductance gradient of the system, which shows that the proposed analytical method of calculating the dynamic inductance gradient is correct, and it also provides certain references to the design optimization of the electromagnetic orbit launchers.

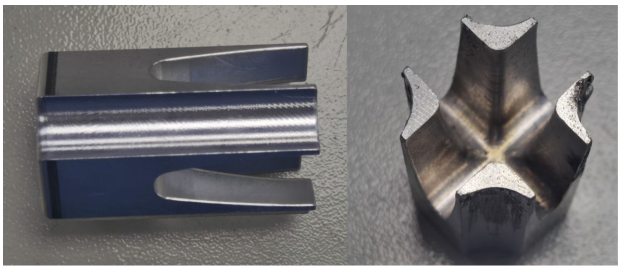

FIGURE 2. Physical drawing of armature.

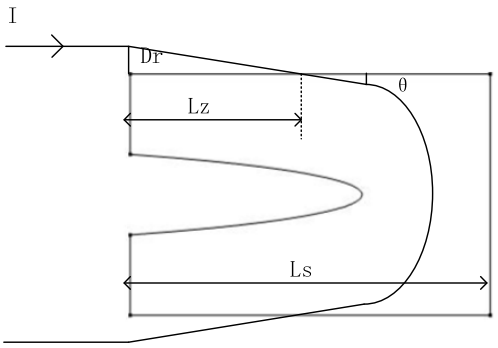

FIGURE 3. Schematic diagram of the current area on the armature.

II. CONSTRUCTION OF AN EQUIVALENT GEOMETRIC MODEL BASED ON SKINNING DEPTH

A. MODELING OF DYNAMIC ELECTRICAL LAUNCHING

The three-dimensional model of the series enhanced four-rail electromagnetic launcher is shown in Figure 1

The primary and backfield augmentation rails are connected in series and share a common power system. Current is fed from the two opposite enhancement rails and flows through the armature from the pair of main rails in the perpendicular direction, making a closed loop of the eight main and secondary rails and the armature. The pulsed current generates a magnetic flux density B in the cavity, and the current on the armature is subjected to a Lorentz force Fa in the magnetic field, which drives the armature in the +Z direction with velocity v.

The four-rail armature model is shown in Fig. 2.

Rotate Figure 1 45° clockwise around the Y-axis to take a 2D model of the YOZ planar armature, a simplified model of the current on the armature is shown in Fig. 3.

Ls is the armature length, θ is the angle of current inflow into the armature, Dr is the current skinning depth of the rail, and Lz is the range of current inflow at the armature-rail interface from the z-direction.

Diffusion equation for the magnetic field in orbit:

$$\frac{1}{\mu_0\sigma_r}\left(\frac{\partial^2 B_r}{\partial x^2}+\frac{\partial^2 B_r}{\partial y^2}+\frac{\partial^2 B_r}{\partial z^2}\right)=\frac{\partial B_r}{\partial t} \tag{1}$$

In the above equation μ_0 is the vacuum permeability, B_r is the magnetic flux density inside the rail, and σ_r is the conductivity of the rail material.

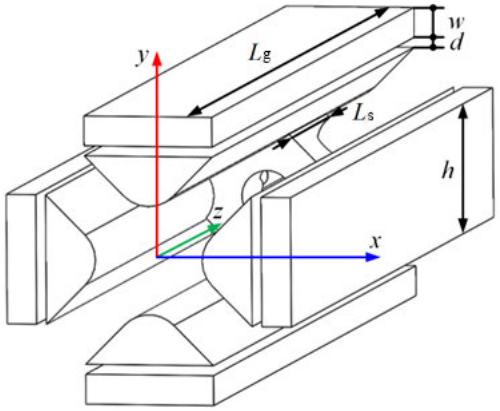

FIGURE 4. Schematic diagram of armature movement.

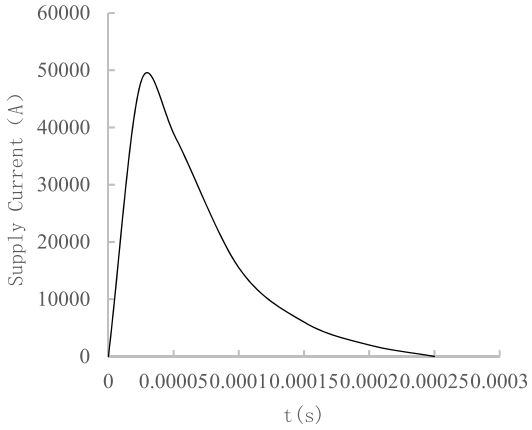

FIGURE 5. Power discharge waveform.

The four rails of the four-rail electromagnetic launcher are distributed in a 90° circular array around the armature, starting from the top in clockwise direction as rails 1, 2, 3, and 4. Taking the quarter model as the object of study, the magnetic field changes faster in the y-direction and ignores the magnetic field changes in the x- and z-directions for rails 1 and 3, and the magnetic field changes faster in the x-direction and ignores the magnetic field changes in the y- and z-directions for rails 2 and 4. A simplified equation for the diffusion of the magnetic field in the rail is obtained:

$$\begin{cases} \dfrac{1}{\mu_0\sigma_r}\dfrac{\partial^2 B_{r1,3}}{\partial y^2} = \dfrac{\partial B_{r1,3}}{\partial t} \\ \dfrac{1}{\mu_0\sigma_r}\dfrac{\partial^2 B_{r2,4}}{\partial x^2} = \dfrac{\partial B_{r2,4}}{\partial t} \end{cases} \tag{2}$$

The armature moves along the Z-axis at a high speed on the rail, when the movement distance is ΔZ as shown in Fig. 4, at this time the magnetic field diffusion equation in the rail is as follows:

$$\begin{cases} \dfrac{1}{\mu_0\sigma_r}\dfrac{\partial^2 B_{r1,3}}{\partial y^2} = v\dfrac{\partial B_{r1,3}}{\partial(\Delta z)} \\ \dfrac{1}{\mu_0\sigma_r}\dfrac{\partial^2 B_{r2,4}}{\partial x^2} = v\dfrac{\partial B_{r2,4}}{\partial(\Delta z)} \end{cases} \tag{3}$$

Based on the boundary conditions of the armature of the electromagnetic rail launcher in the literature [13], the boundary conditions of the four-rail electromagnetic launcher are set as follows:

$$\begin{cases} B_a(x, y, z_a) = B_0 + B_{out} \\ \left.\dfrac{\partial B_a}{\partial y}\right|_{y=-\frac{k}{2}} = 0 \\ B_a(x, y, z_a + L_s) = B_{out} \end{cases} \tag{4}$$

In the above equation, B_a is the magnetic flux density on the armature, B_0 is the magnetic flux density generated by the current in the tail of the armature, and B_{out} is the magnetic flux density of the enhancement rail on the armature. The enhancement rail current distribution is not affected by armature motion, so B_{out} does not change with armature motion. k is the spacing of a set of relative inner rails.

The armature moves along the Z-axis at a high speed on the rail, and when the movement distance is ΔZ, let the current density at the tail of the armature be J_0,the inner rails 1 and 3 and the inner rails 2 and 4, the current densities decay in the Y- and X-directions, respectively, as follows:

$$\begin{cases} J_{ay} = -J_0 e^{-\Delta z/L_z} \\ J_{ax} = -J_0 e^{-\Delta z/L_z} \end{cases} \tag{5}$$

From the Ampere's loop theorem, the current in the rail when the armature moves to ΔZ produces the magnetic flux density on the armature as follows:

$$B_{a1}(\Delta z) = -\mu_0 \int J_{ay} d(\Delta z) - \mu_0 \int J_{ax} d(\Delta z) \tag{6}$$

Equation (6) of equation (5) yields:

$$B(\Delta z) = B_0\left[e^{-\Delta z/L_Z} - \frac{\Delta z}{L} e^{-L_s/L_Z}\right] + B_{out} \tag{7}$$

B. RAIL SKINNING DEPTH MODELING

Figure 5 shows the actual current waveform obtained by the current acquisition system in the experimental setup, from the figure we can get the armature discharge time is about 0.25ms, the current wave model can be approximated as a sawtooth wave, and according to the literature [14], its frequency can be regarded as 1/2 sine wave.

Literature [15] demonstrates that the current skin depth effect is the dominant factor when the armature speed is below the critical speed of 150 m/s. At this time the rail skin depth is as follows:

$$\delta_1 = \sqrt{\frac{1}{\pi\mu_0\sigma_r f}} \tag{8}$$

In the above equation f is the current frequency, the power supply frequency of this experimental platform is 2kHz as shown in Fig. 5.

When the armature speed exceeds the critical speed, the velocity skin effect is the dominant factor, taking the average current density along the z and y directions of the main rail,

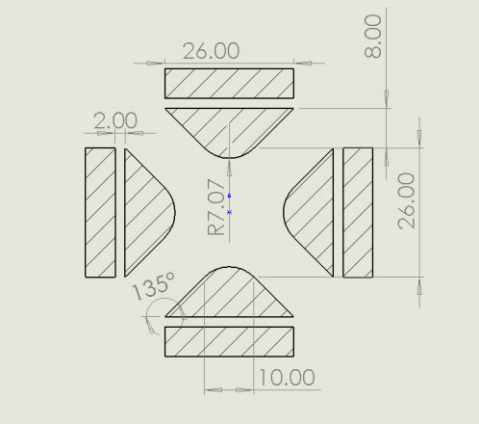

FIGURE 6. Primary and secondary rail parameters.

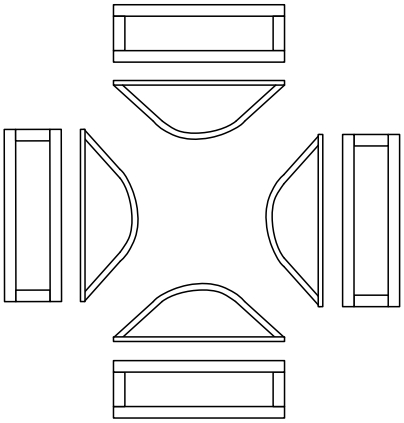

FIGURE 7. Equivalent geometric model of main and secondary rails.

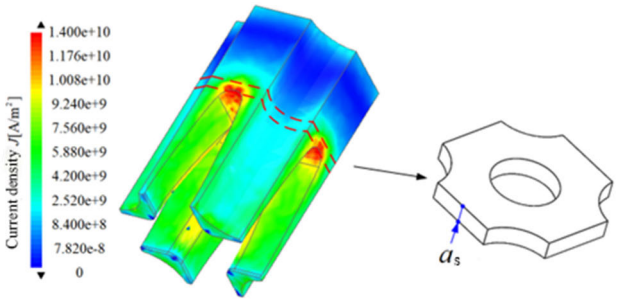

FIGURE 8. Simplified model of armature (axial).

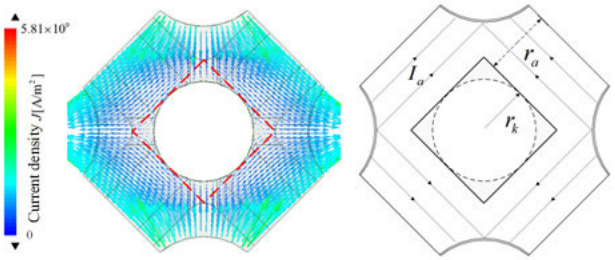

FIGURE 9. Armature current simplification [8].

combined with the geometric relationship in Fig. 3 can be obtained as follows:

$$\tan\theta = \frac{-\mathbf{J}_{\mathrm{ry}}}{\mathbf{J}_{\mathrm{rz}}} = \frac{L_{\mathrm{z}}}{D_{\mathrm{r}}} \tag{9}$$

The solution of the equation of type (3) is as follows:

$$B_{\mathrm{r}} = \int_0^{\Delta z} \frac{dB_{\mathrm{i}}(\xi)}{d\xi} erfc\left\{\frac{y}{2\left[\mu_0\delta_{\mathrm{r}}v\left(\Delta z-\xi\right)\right]^{1/2}}\right\} d\xi \tag{10}$$

Equations (9) and (10) are solved for:

$$\begin{cases} \delta_2 = \dfrac{1}{1.21^2\tan\theta}\cdot\dfrac{1}{\mu_0\sigma_{\mathrm{r}}v} \\ \tan\theta = 1.21\sqrt{\dfrac{1}{\mu_0\sigma_{\mathrm{r}}v\pi^2L_{\mathrm{z}}}} \end{cases} \tag{11}$$

The skinning depth of the current in the inner orbit is as follows:

$$\delta_2 = \frac{1.21^3}{\sqrt{\mu_0\sigma_{\mathrm{r}}\frac{v}{L_{\mathrm{z}}}}} = \sqrt{\frac{1}{\pi\mu_0\sigma_{\mathrm{r}}\frac{v}{\pi^2L_{\mathrm{z}}}}} \tag{12}$$

Summarizing the equivalent convergent skin depth δ is as follows:

$$\begin{cases} \delta_1 = \sqrt{\dfrac{1}{\pi\mu_0\sigma_{\mathrm{r}}f}} \quad \ldots\ldots\ldots\ldots\ldots\ldots v \le v_c \\ \delta_2 = \sqrt{\dfrac{1}{\pi\mu_0\sigma_{\mathrm{r}}\frac{v}{\pi^2L_{\mathrm{s}}}}} \quad \ldots\ldots\ldots\ldots v > v_c \end{cases} \tag{13}$$

where $L_Z = \kappa L_{\mathrm{s}}$, κ is the scaling factor, take the armature length $L_{\mathrm{s}} = 40mm$, frequency $f = 2\mathrm{kHz}$, when $v = v_{\mathrm{c}}$, from the equation (13) solved. $\kappa = 0.1899$.

C. EQUIVALENT MOLD GEOMETRY MODELING

Set the backfield enhancement rail height $h = 26\mathrm{mm}$, enhancement rail thickness $w = 6\mathrm{mm}$, main and vice rail spacing $d = 2\mathrm{mm}$; convex rail bottom length $h = 26\mathrm{mm}$, waist length $h_2 = 8\sqrt{2}\mathrm{mm}$, and armature contact part of the arc radius is $R = 7.07\mathrm{mm}$. the main and vice rails are shown in Fig. 6.

The equivalent geometric model of the rail based on the skinning depth is shown in Fig. 7.

Where the primary rail skinning depth is δ_{in} and the secondary rail skinning depth is δ_{out}. The current has a cross-sectional area of s_1 in the ith primary rail skinning layer and s_2 in the ith secondary rail skinning layer.

$$\begin{cases} s_1 = \delta_{\mathrm{in}}\left(2h_2 - 2\delta_{\mathrm{in}}\right) + \dfrac{\pi\delta_{\mathrm{in}}}{4}\left(2R - \delta_{\mathrm{in}}\right) + h\delta_{\mathrm{in}} \\ s_2 = 2h\delta_{\mathrm{out}} + 2\delta_{\mathrm{out}}\left(w - 2\delta_{\mathrm{out}}\right) \end{cases} \tag{14}$$

Armature in the launch process armature wall current mainly produces lateral force, armature head current produces Z-direction electromagnetic force, by Biot-Savart Law can be obtained, the inductance gradient is mainly affected by the armature head current, so in the case of not affecting the reflection of the actual launch to simplify the theoretical derivation, the armature head is selected to analyze the modeling, as shown in Figure 8.

Four-rail electromagnetic launcher in the chamber axis magnetic field offset and the current in the armature is centrosymmetric distribution, so the armature current I_a is equal to $I/2$, based on the convergence of the skin depth to establish an equivalent model is shown in Figure 9.

The armature cross-section current density is as follows:

$$J = \frac{I}{2}(r_a \cdot a_s) \tag{15}$$

III. COMPUTATIONAL ANALYSIS OF DYNAMIC INDUCTANCE GRADIENT

A. ANALYTICAL METHOD TO CALCULATE DYNAMIC INDUCTANCE GRADIENT

Backfield-enhanced four-rail electromagnetic launcher in the launch process, the armature is driven by the Z-direction electromagnetic force F_z, due to the four sets of rails to the center of the symmetric distribution, and connected in series, so find a main rail on the armature thrust F_{in} and the corresponding backfield-enhanced rail on the armature thrust F_{out}, can be found in the total thrust.

$$F_Z = \sum_{i=1}^{4}(F_{ini} + F_{outi}) \tag{16}$$

Also known as:

$$F_Z = \frac{1}{2}L^v I^2 \tag{17}$$

where L^v is the system dynamic inductance gradient of the backfield-enhanced four-rail electromagnetic launcher.

The final system dynamic inductance gradient is as follows:

$$L^v = \frac{2F_Z}{I^2} \tag{18}$$

In the following, the analytical formula for the dynamic inductance gradient of the enhanced four-rail electromagnetic launcher is derived according to the Biot-Savart Law. Setting a point P(α, β, γ) on the armature, the current inside the skin layer is regarded as a uniformly distributed line current under the consideration of skinning effect, from which the line current element Idl inside the rail generates the magnetic flux density at point P as follows:

$$dB = \frac{\mu_0}{4\pi}\frac{Idl \times \mathbf{r}}{|\mathbf{r}|^3} \tag{19}$$

where: l is the length of the energized conductor; r is the distance vector from the current element Idl to point P.

As shown in Fig. 1 the current flows along the Z-axis within the rail, then the current source at any point on the main rail 1 can be expressed as $(I/S_1)dxdyk$,where $\boldsymbol{i}, \boldsymbol{j}, \boldsymbol{k}$ are the unit vectors in the X,Y,Z axes, respectively. The joint equations (14) and (19) yield the magnetic field strength of the main rail i-th at point P on the armature as follows:

$$dB_{in1} = \frac{\mu_0}{4\pi}\frac{Idxdy\mathbf{k} \times \mathbf{r}}{|\mathbf{r}|^3\left[\delta_{in}(2h_2 - 2\delta_{in}) + \frac{\pi\delta_{in}}{4}(2R - \delta_{in}) + h\delta_{in}\right]} \tag{20}$$

Since the current element is infinitesimal, the coordinates of the center point of the current element to the P-point vector is taken as the vector of the current element to the P-point with the following equation.

$$\mathbf{r} = (x - a)\,\mathbf{i} + (y - \beta)\,\mathbf{j} + (z - \gamma)\,\mathbf{k} \tag{21}$$

$$|\mathbf{r}| = \sqrt{(x - \alpha)^2 + (y - \beta)^2 + (z - \gamma)^2} \tag{22}$$

Bringing Eq. (20) Eq. (21) into Eq. (19) yields:

$$dB_{in1} = \frac{\mu_0}{4\pi}\frac{Idxdy\left[(x - \alpha)\,\mathbf{k} \times \mathbf{i} + (y - \beta)\,\mathbf{k} \times \mathbf{j}\right]}{|\mathbf{r}|^3\left[\delta_{in}(2h_2 - 2\delta_{in}) + \frac{\pi\delta_{in}}{4}(2R - \delta_{in}) + h\delta_{in}\right]} \tag{23}$$

Integrate Eq. (23) to find the magnetic flux density generated by the current in the main orbit 1 at point P:

$$B_{in1} = \frac{\mu_0}{4\pi}\frac{I\iint_{S_1}\left[(x - \alpha)\,\mathbf{k} \times \mathbf{i} + (y - \beta)\,\mathbf{k} \times \mathbf{j}\right]dxdy}{|\mathbf{r}|^3\left[\delta_{in}(2h_2 - 2\delta_{in}) + \frac{\pi\delta_{in}}{4}(2R - \delta_{in}) + h\delta_{in}\right]} \tag{24}$$

Because of the four groups of rails into a 90-degree circumferential array of series distribution, so the other main rail at the P point produces the same size of the magnetic flux density only different direction. By the principle of magnetic field superposition, the magnetic flux density generated by the currents in the four main rails at point P is as follows:

$$B_{in} = \frac{\mu_0 I}{4\pi}\sum_{i=1}^{4} \times \frac{(-1)^{i+1}\iint_{S_1}\left[(x - \alpha)\,\mathbf{k} \times \mathbf{i} + (y - \beta)\,\mathbf{k} \times \mathbf{j}\right]dxdy}{|\mathbf{r}|^3\left[\delta_{in}(2h_2 - 2\delta_{in}) + \frac{\pi\delta_{in}}{4}(2R - \delta_{in}) + h\delta_{in}\right]} \tag{25}$$

The backfield enhancement rails are only affected by the current skinning effect, the skinning depth is δ_{out}, and the cross-sectional area of the skinned layer of the secondary rails is s_2. Derived from Eq. (24), the flux densities of the four enhancement rails for any point in the gun chamber are as follows:

$$B_{out} = \frac{\mu_0 I}{4\pi}\sum_{i=1}^{4} \times \frac{(-1)^{i+1}\iint_{S_2}\left[(x - \alpha)\,\mathbf{k} \times \mathbf{i} + (y - \beta)\,\mathbf{k} \times \mathbf{j}\right]dxdy}{|\mathbf{r}|^3\left[2h\delta_{out} + 2\delta_{out}(w - 2\delta_{out})\right]} \tag{26}$$

The armature is subjected to electromagnetic thrust as follows:

$$F_z = \sum_{i=1}^{4}(F_{ini} + F_{outi})$$

TABLE 1. Statistical results of initial contact parameters.

Parameter	Meaning	Numerical value
h	Rail height	26mm
w	Enhanced rail thickness	6mm
d	Enhanced rail to main rail distance	2mm
h_2	Main rail waist length	$8\sqrt{2}$ mm
R	Radius of main guide projection	7.07mm
r_a	Effective armature width	6.855mm
r_k	Armature inner diameter	5.175mm
L_g	Length of guide rails	380mm
L_s	Armature thickness	40mm
f	Current frequency	2000Hz
I	Amount of current	50kA

$$= \sum_{i=1}^{4} \left(\int B_{ini} J \times dl + \int B_{outi} J \times dl \right) \tag{27}$$

Equation (13) Eq. (14) Eq. (18) Eq. (27) solves the dynamic inductance gradient of the enhanced electromagnetic launcher as:

$$L^v = \frac{\mu_0 I^3}{8\pi |\mathbf{r}|^3} \sum_{i=1}^{4} (-1)^{i+1} \left[\frac{\iint_{S_1} \mathbf{k} \times \mathbf{r} dxdy}{S_1} + \frac{\iint_{S_2} \mathbf{k} \times \mathbf{r} dxdy}{S_2} \right] \tag{28}$$

where the effective cross-section S is a function of the speed of armature motion, and the link between the speed of armature motion and the inductance gradient of the system is established through the effective cross-section area.

B. VORTEX FIELD SIMULATION CALCULATION

In this section, the armature rail modeling is simulated in the vortex field, and the inductance gradient is calculated accurately by considering the influence of skinning effect as a control to verify the accuracy of the analytical method. According to the principle of virtual work [16], assuming that the armature motion in the chamber is only subject to electromagnetic inference in the Z direction and the virtual displacement is dz, the following equation is obtained through the law of energy conservation.

$$dW_z = dW_f + dW_s + dW_m \tag{29}$$

In the above formula: is the power supply to the total energy of the system, is the electromagnetic force to push the armature to do the work, is to the field outside the loss of energy; is the magnetic field energy increment. In the instantaneous work process, dz takes a very small value, the total energy of the system is considered to be all used in the electromagnetic force to push the armature movement, namely:

$$dW_z = dW_f \tag{30}$$

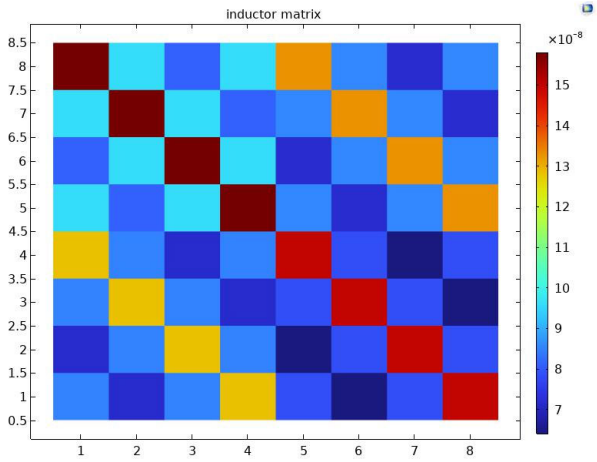

FIGURE 10. Inductance matrix simulation results.

TABLE 2. Simulation of inductance gradient.

Armature position(mm)	Simulation of inductance gradient ($\mu H \cdot m^{-1}$)
60	1.4697
100	1.4594
140	1.4583
180	1.4571
220	1.4566
260	1.4557
300	1.4553

included among these:

$$dW_f = F_z dz \tag{31}$$

$$F_z = \frac{1}{2} L' I^2 \tag{32}$$

Equation (30) (31) (32) gives:

$$L' = \frac{2dW_z}{I^2 dz} \tag{33}$$

The total energy is obtained by simulation and combined with Eq. (33) to obtain the average inductance gradient of the armature movement for a very short time, and this average inductance gradient is used as the instantaneous inductance gradient at the location of the armature.

A specific series-enhanced four-rail electromagnetic launcher model is selected to calculate the inductance gradient using analytical method and eddy current field simulation, respectively. The parameters of the selected example model are shown in Table 1 below:

The rail material is chrome zirconium copper with density $8.66\times10^3 kg\cdot m^{-3}$, vacuum permeability $1.2566 \times 10^{-6} H\cdot m^{-1}$, conductivity $5.8\times10^7 S\cdot m^{-1}$, resistivity $5.4 \times 10^{-8} kg\cdot m^{-3}$. The armature material is 6061 aluminum with density $2.698\times10^3 kg\cdot m^{-3}$, vacuum permeability $1.2566 \times 10^{-6} H\cdot m^{-1}$, conductivity $3.76\times10^7 S\cdot m^{-1}$, resistivity $2.7 \times 10^{-8} kg\cdot m^{-3}$. The peak excitation pulse current is 50kA and the frequency is 2000Hz.

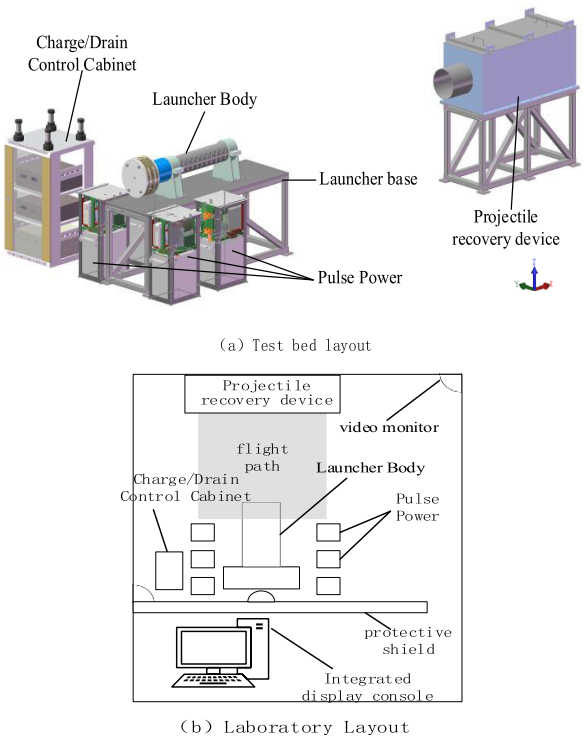

FIGURE 11. Block diagram of system components.

Considering the case of no armature, simulation calculations are carried out using COMSOL, the obtained inductance matrix table is plotted using a 2D plotting group and the visualization of the inductance matrix is obtained as shown in Fig. 10, where the diagonal entries are self-inductive, and will be non-diagonal entries for mutual inductance. The inductance gradient of the system without armature is found to be 1.3599 μH/m through equation (33).

The inductance gradients were calculated using eddy current field simulation for armature movement to 60m, 100mm, 140mm, 180mm, 220mm, 260mm and 300mm respectively. Setting 0mm at the end of the armature as the relative zero-energy position, the system inductance gradient at these seven positions is calculated by combining with equation (33). The recorded results are shown in Table 2 below.

The armature speed in the analytical method is measured by building a test rig to measure the instantaneous speed at seven positions, and the armature speed is measured using B-dot probes.

IV. SOME COMMON MISTAKES

Build a test platform to measure the armature motion velocity, solve the dynamic inductance gradient of the system by analytical method, and compare and analyze the results with the eddy current field calculations.

A. TEST PLATFORM

The series-enhanced four-rail electromagnetic launch test platform is equipped with the functions of voltage boosting, electric energy storage, control triggering, high-current pulse network formation, armature propulsion, data acquisition and armature interception and recovery. The overall system has the functions of four-rail electromagnetic launch system experiment demonstration and parameter acquisition and uploading.

The four-rail electromagnetic launch system is mainly composed of power supply system, control system, acquisition system and launch system. In the armature launch test

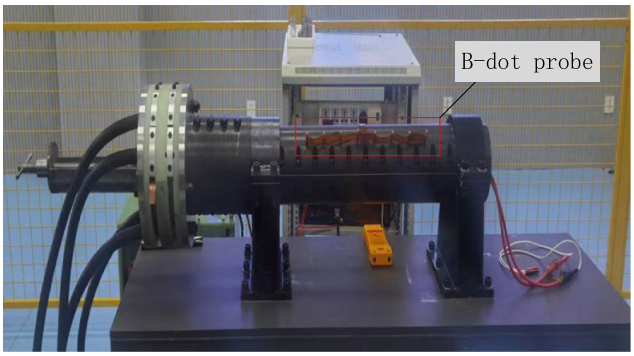

FIGURE 12. Velocimetry equipment under test.

FIGURE 13. The moment the armature is discharged.

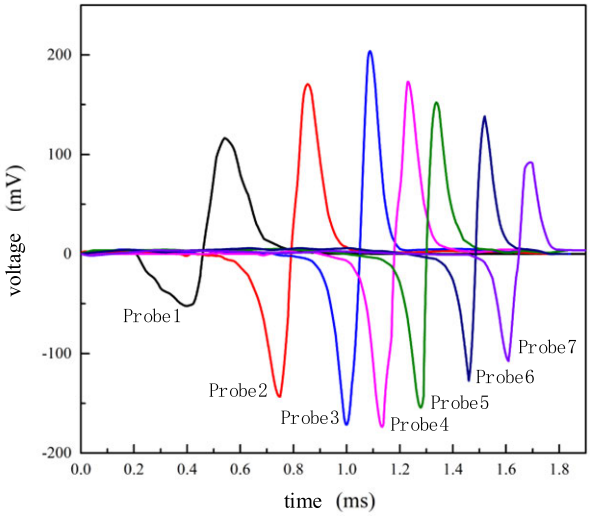

FIGURE 14. B-dot probe measurement results.

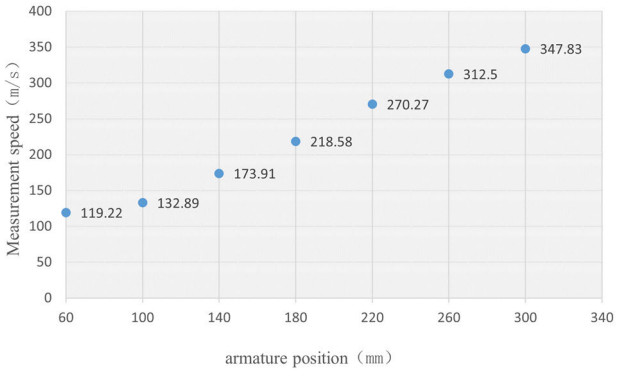

FIGURE 15. Armature speed.

TABLE 3. Analytic calculation of inductance gradient.

Armature position(mm)	Analytic calculation of inductance gradient ($\mu H \cdot m^{-1}$)
60	1.439
100	1.4291
140	1.4219
180	1.4067
220	1.3985
260	1.3882
300	1.3868

process will produce high voltage and strong magnetic field, need to design a reasonable laboratory layout to ensure that the equipment works properly while ensuring the safety of personnel and equipment. Figure 11 shows the overall layout of the electromagnetic launch experiment.

B. VELOCIMETRY TEST

The B-dot probe [17] converts the change in magnetic field caused by the armature passing into an induced voltage, which in turn records the moment the armature passes the probe. The interval between the measurement points is small enough to consider that the armature passes through the two measurement points with a uniform speed at the instantaneous time, and the average speed of the armature between the two probes is the instantaneous speed of the armature. The test was conducted by mounting seven B-dot probes equidistant 40 mm apart. Figure 12 shows the velocity measuring element and its mounting position on the test rig.

Figure 13 shows the moment of armature exit for the launch test. Since the current is still present in the rail when the armature exits, the armature will arc as it leaves the launcher, consuming the remaining current in the rail.

Figure 14 shows the waveform of the induced voltage measured by the B-dot probe, and the moment of zero voltage is the moment when the armature reaches the corresponding B-dot probe position. Figure 15 shows the experimentally measured speed of the armature after 7 positions.

C. COMPARATIVE ANALSIS OF THE TWO CALCULATION METHODS

The inductance gradients were calculated using the analytical method for armature movement to 60m, 100mm, 140mm, 180mm, 220mm, 260mm and 300mm respectively. Substitute the armature speed in Table 3 into Eq. (28) to find the inductance gradient of the system when the armature is in these 7 positions. The recorded results are shown in Table 3 below.

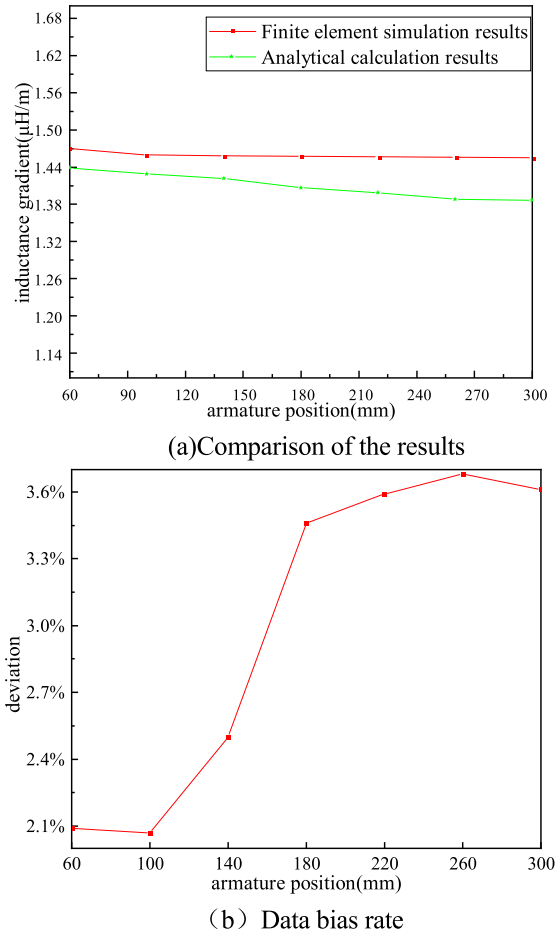

FIGURE 16. Comparison of the results of the two calculation methods.

A comparison of the results of the two calculation methods is shown in Figure 16a below, and the data deviation rate is shown in Figure 16b (the deviation rate is the difference between the results of the simulation calculation method and the results of the analytical calculation method divided by the simulation value) is 2.09% at 60 mm, 2.07% at 100 mm, 2.5% at 140 mm, 3.46% at 180 mm, 3.59% at 220 mm, 3.68% at 260mm, 3.61% at 300mm.

From Fig. 16a, it can be seen that the inductance gradient tends to decrease gradually as the armature moves on the rail toward the tail of the electrical launching. It shows that the armature is located in different positions has different effects on the inductance gradient of the electromagnetic launcher, and the farther the armature movement position is, and the longer the length of the rail in the access circuit is, the smaller the effect is. The trend of the analytical method and the simulation results are the same, and the deviation rate is not more than 3.68%, which basically meets the requirements of calculation accuracy.

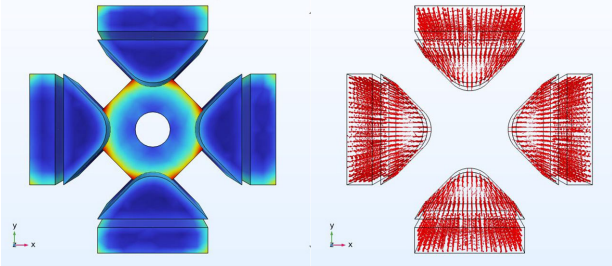

（a） Current density distribution at 180 mm without considering velocity effects

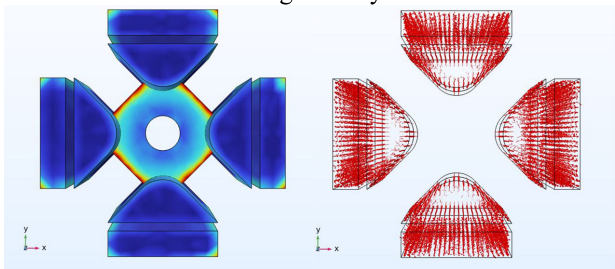

（b） Current density distribution considering velocity effects at 180mm

FIGURE 17. Current density distribution cloud.

As shown in Figure 16b, the values calculated by the analytical method are smaller than the simulation values, and the deviation rates calculated by the two methods for the armature at 60mm and 100mm are relatively similar. The deviation rate of the data at 140mm increases by 2.5%, compared to the increase of 19.6% compared to 100mm. The deviation rate of the data at 180mm of the armature further increases, compared to the increase of 38.4% compared to 140mm. The error rate changes tend to be gentle at 220mm, 260mm, and 300mm.

Explained in the armature at 60mm and 100mm speed less than 150m/s, the current distribution is mainly affected by the current skinning effect, skinning depth of 1.4531mm, the data deviation is mainly due to the principle of virtual work that all the energy is used to drive the armature along the rail movement, ignoring the energy loss and the magnetic field energy conversion. In the armature is located in 140mm at the instantaneous speed of 173.91m/s. At this time by the speed of skinning influence, the main rail current tends to the rail surface more and more, the distribution of current density in the rail directly affects the size and distribution of magnetic induction intensity B in the chamber, which in turn affects the storage energy of the magnetic field in the space as well as the corresponding inductance coefficient. The higher the armature speed, the thinner the thickness of the main rail skin layer, the smaller the dynamic inductance gradient. In the armature located at 180 mm armature speed reaches 218.58 m/s, the skin depth is smaller for 1.1865 mm, resulting in a further increase in the deviation rate from the simulation calculated value, as shown in Fig. 17, considering the speed effect of the skin depth smaller.

When the armature is located at 220mm at a speed of 270.27m/s, the deviation rate changes are small, the current is distributed on the main rail surface, and the effect of the skin layer thickness change on the magnetic induction intensity distribution is weakened. When the armature speed is 312.5m/s and 347.83m/s at armature located at 260mm and 300mm respectively. Corresponding to the deviation rate of 3.68% and 3.61%, with the armature speed increasing, the current is more and more concentrated in the rail surface and the skinning depth is gradually stabilized, so the inductance gradient is gradually reduced and stabilized.

The analytical method takes into account the effect of armature motion, which more accurately reflects the inductance gradient change during the firing process compared to the eddy current field simulation.

V. CONCLUSION

In this paper, the dynamic inductance gradient of a series-enhanced four-rail electromagnetic launcher is derived from the Biot-Savart Law, taking into account the effect of armature speed on the inductance gradient. Since the current density and magnetic induction strength on the rail are dynamically changing during the armature launching process, the analytical method proposed in this paper to calculate the dynamic inductance gradient can more accurately reflect the actual situation during the launching process.

The following conclusions are obtained through the comparative analysis of eddy current field simulation:

(1)Under the consideration of the influence of armature motion on the inductance gradient of the series-enhanced four-rail electromagnetic launcher, the calculation results of the analytical method deduced in this paper can more accurately reflect the change of the inductance gradient in the launching process.

(2)The initial stage of armature launching speed is small, the rail current distribution is affected by the current skin effect related to the current frequency, and as the armature speed is increased, the current distribution is affected by the velocity skin effect, and the skin depth decreases.

(3)When the armature speed is greater than 312.5m/s, the dynamic inductance gradient gradually decreases and stabilizes as the armature speed increases. This law is consistent with the Kerrisk high-frequency inductance gradient law.

REFERENCES

[1] W. Ma, J. Lu, and X. Li, "Electromagnetic launch hypervelocity integrated projectile," *J. Nat. Univ. Defense Technol.*, vol. 41, no. 4, pp. 1–10, Dec. 2019.

[2] V. Vertelis, G. Vincent, M. Schneider, S. Balevicius, V. Stankevic, and N. Žurauskiene, "Magnetic field expulsion from a conducting projectile in a pulsed serial augmented railgun," *IEEE Trans. Plasma Sci.*, vol. 48, no. 3, pp. 727–732, Mar. 2020.

[3] J. W. Zhang, J. Y. Lu, and S. Tan, "Research status of damage in rails for electromagnetic launchers," *Acta Armamentarii*, vol. 44, no. 7, p. 19, 2023.

[4] T. D. Li, G. Feng, and S. W. Liu, "Analysis of electromagnetic characteristics of orbits of series-enhanced four-rail electromagnetic launcher," *Fire Control Command Control*, vol. 46, no. 9, pp. 56–61, 2021.

[5] J. N. Snyder and F. C. Grover, "Inductance calculations working formulas and tables," *Math. Comput.*, vol. 18, no. 85, p. 164, Jan. 1964.

[6] J. F. Kerrisk, "Current distribution and inductance calculations for rail-gun conductors," NASA, Washington, DC, USA, Tech. Rep. 82, 1981.

[7] T. Li, G. Feng, Z. Lian, and S. Liu, "Simulation analysis of inductance gradient of series enhanced four-rail electromagnetic launcher," *J. Phys., Conf. Ser.*, vol. 1678, no. 1, Nov. 2020, Art. no. 012052.
[8] S. Ren, G. Feng, P. Zhang, T. Li, and X. Zhao, "Method of calculating inductance gradient for complex electromagnetic rail launcher," *Electronics*, vol. 11, no. 18, p. 2912, Sep. 2022.
[9] Z. Peng, G. Wang, X. Zhai, and X. Zhang, "Modeling and analysis of time-varying inductance gradient for electromagnetic rail launcher," *Trans. China Electrotech. Soc.*, vol. 35, no. 23, pp. 4843–4851, 2020.
[10] X. Zhai, X. Li, H. Liu, and Z. Peng, "Analysis of dynamic inductance gradient of electromagnetic rail launcher," *J. Nat. Univ. Defense Technol.*, vol. 44, no. 3, pp. 156–163, 2022.
[11] M. Ghassemi, Y. M. Barsi, and M. H. Hamedi, "Analysis of force distribution acting upon the rails and the armature and prediction of velocity with time in an electromagnetic launcher with new method," *IEEE Trans. Magn.*, vol. 43, no. 1, pp. 132–136, Jan. 2007.
[12] X. Li, J. Lu, Y. Li, and X. Wu, "Analysis of distribution characteristics of in-bore magnetic field of electromagnetically launched projectile based on analytical method," *Acta Armamentarii*, vol. 37, no. 12, pp. 2205–2211, 2016.
[13] T. Ling-Ling and L. I. Hao-Jie, "Simulation analysis of railgun in-bore high magnetic field," *Comput. Simul.*, vol. 31, no. 11, pp. 1–5, 2014.
[14] Q.-A. Lv, H.-J. Xiang, B. Lei, Q. Zhang, K.-Y. Zhao, Z.-Y. Li, and Y.-C. Xing, "Physical principle and relevant restraining methods about velocity skin effect," *IEEE Trans. Plasma Sci.*, vol. 43, no. 5, pp. 1523–1530, May 2015.
[15] Z. Wang, L. Chen, P. You, X. Lan, and Y. Ge, "Current distribution characteristics of armature-rail interface under velocity skin effect and contact resistance," *Trans. China Electrotech. Soc.*, vol. 37, no. 19, pp. 5003–5010, 2022.
[16] S. Y. Tong, G. Feng, and Z. M. Lian, "Analysis of factors affecting inductance gradient of four-rail electromagnetic launcher analysis of factors affecting inductance gradient of four-rail electromagnetic launcher," *J. Ordnance Equip. Eng.*, vol. 40, no. 12, pp. 221–224, 2019.
[17] S. Song and C. Cheng, "Measurement of solid Armature's in-bore velocity using B-dot probes in a series-augmented railguns," *IEEE Trans. Plasma Sci.*, vol. 43, no. 5, pp. 1310–1315, May 2015.

BO-LIN CAI was born in Shaanxi, China, in 1996. He is currently pursuing the master's degree in the theory of electromagnetic launch technology with Air Force Engineering University, Xi'an, China. His current research interests include the theory of electromagnetic rail launchers and numerical analysis of electromagnetic fields.

GANG FENG was born in Shaanxi, China, in 1976. He received the M.S. degree in weapons from Air Force Engineering University, Xi'an, China. He is currently an Associate Professor with the Air and Missile Defense College, Air Force Engineering University. His current research interest includes the theory and technology of weapons.

KE-FENG YANG was born in Sichuan, China, in 2001. He is currently pursuing the master's degree in the theory of electromagnetic launch technology with Air Force Engineering University, Xi'an, China. His current research interest includes theory and technology of weapon systems.